Time-Series Deformation Monitoring over the Kalush-Golynsk Potassium Salt Deposit (Ukraine), Using InSAR Method

Kukhtar, D.,* Dorosh, L. and Hrynishak, M.
Department of Geodesy and Land Management, Ivano-Frankivsk National Technical University of Oil and Gas, Ivano-Frankivsk, Ukraine
E-mail: denys.kukhtar@nung.edu.ua,* liubov.dorosh@gmail.com, nikolaygrynishak@gmail.com
Corresponding Author

DOI: https://doi.org/10.52939/ijg.v22i4.4936

Abstract
Improper liquidation of underground mine cavities can lead to the development of hazardous geodynamic processes, including progressive surface subsidence and ground instability in mining regions. This study demonstrates a workflow for satellite radar monitoring of deformation processes in mining regions using Sentinel-1 SAR data. Time-series analysis was performed using the NSBAS (New Small Baseline Subset) method implemented in the MintPy software package. Interferogram generation was automated through the HyP3 cloud processing platform of the Alaska Satellite Facility, while subsequent analysis was conducted in the Jupyter Notebook environment provided by the OpenSARlab platform. A total of 295 interferometric pairs covering the period from April 2021, to March 2024 were analyzed. Tropospheric delay corrections were introduced using ERA5 atmospheric reanalysis data distributed via the Climate Data Store service. The resulting mean velocity map reveals several zones of intensive subsidence within the Novo-Holyn mining field, including the area of a large sinkhole currently flooded with water, the roof of a reclaimed tailings storage facility, and parts of the nearby residential area. In some locations, deformation rates approach 50 cm/year, indicating rapid surface destabilization related to underground mining processes. To validate the InSAR results, four annual campaigns of high-precision second-order levelling were conducted. A comparison of deformation rates along four levelling profiles shows good agreement between satellite radar monitoring and ground-based geodetic measurements. The presented approach demonstrates that time-series InSAR analysis with short temporal baselines can provide reliable deformation estimates even under conditions of rapid subsidence and strong temporal decorrelation typical of mining areas. The proposed processing workflow can therefore be applied to other regions affected by underground mining or similar geodynamic processes, expanding the practical capabilities of satellite radar monitoring for early detection and localization of hazardous surface deformation.

Keywords: HyP3, Levelling, Mining Field, MintPy, NSBAS, Subsidence

1. Introduction

The observations of modern geodynamic movements of the Earth play a significant role in preventing natural and technogenic disasters. Most often, an object of such observations is the territories where mineral extraction is conducted. In many regions of the world, deformations of the Earth's surface occur as a result of oil and gas extraction [1][2] and [3], excessive and intensive depletion of aquifers [4][5] [6] and [7], as well as mining activities [8][9][10] and [11]. The measurements of deformation values, which are performed by terrestrial and remote geodetic methods, are carried out to study the peculiarities of deformation processes and control their development. In recent decades, Ukraine's mining enterprises have experienced several major man-made disasters. For instance, in early October 2018, a vault crushed down above the karst surface on the site of enterprise "Polymineral" (Stebnyk, Lviv region). The sinkhole size was 300 meters in diameter and up to 50 meters in depth [12] and [13]. Salt mining activities of the state enterprise "Solotvynskyi Solerudnyk" (Solotvyno, Zakarpattia region) ceased in early 2007. However, this did not stop the ongoing karst processes in the area of the enterprise and beyond. The technogenically activated karst in the area of the Solotvyno rock salt deposit

caused the formation of sinkholes and deformation of the Earth's surface with maximum rates up to 5 cm/year [14] and [15]. Apart from major changes in the terrain, an increased water runoff coefficient can be observed, along with changes in the locations of groundwater recharge and discharge [16]. According to observations, the incorrect decisions regarding the methods of liquidating mine cavities at the Kalush-Holyn potash salt deposit (Kalush, Ivano-Frankivsk region) have led to negative consequences from the impact of underground mining works [17]. As a result, dangerous geodynamic phenomena are in progress on the Earth's surface: formation of sinkholes, landslides, and soil subsidence. These processes occur from time to time and will keep on going with a higher intensity in the future according to experts' predictions [18].

1.1 Study Area

The Kalush-Holyn potash salt deposit is located in the Kalush territorial community and covers an area of about 80 km^2. This deposit started to be developed in 1826. The deposit became a raw material base for the production of mineral fertilizers, technical and food salts, metallic magnesium, caustic soda, vinyl chloride, hydrochloric acid, etc. [19].

The extraction of potassium salts was performed at 3 mines ("Holyn", "Kalush", "Novo-Holyn") [20], as well as by open-pit method at the Dombrovskyi quarry (Figure 1(a)). Nowadays, three mining fields are filled with salt brine including a pulp, two are flooded with saline solutions, two are kept in a "dry conservation". The mines "Holyn", "Kalush", "Novo-Holyn", Dombrovskyi quarry, 2 dumps of saline soils, 2 tailings ponds, and sludge collector of the potash plant are potentially dangerous and can cause subsidence of the Earth's surface, formation of sinkholes, karsts, landslides, pollution of water objects and lands [20]. Since 2020, the subsidence of the Earth's surface over the "Holyn" and "Novo-Holyn" mines has considerably intensified in the area of Kropyvnyk village. The "Novo-Holyn" mine was exploited from 1966 to 1995. As a result of mining activity, 12 million m^3 of underground cavities appeared. In the course of mine liquidation, it was planned to fill the cavities with salt brine. But finally, only half of the mines were filled, while the rest remained dry. In 2020, subsidence occurred outside Kropyvnyk village, covering an area of 6 hectares with a depth of 1 meter. The distance from the funnel to the nearest residential buildings was 300 m. In 2021, a new subsidence in an area of 250×300 meters were recorded. A new funnel appeared 100 m away from residential buildings. The subsidence rate of the Earth's surface reaches 50 cm/year (Figure 1(b)).

Due to the ongoing subsidence and the expanding area of sinkholes, the Municipal Commission on Technogenic and Environmental Safety and Emergencies held a meeting on January 10, 2022. Based on the Commission's decision, the city authorities began preparations for the resettlement of residents whose homes and properties are located in the danger zone.

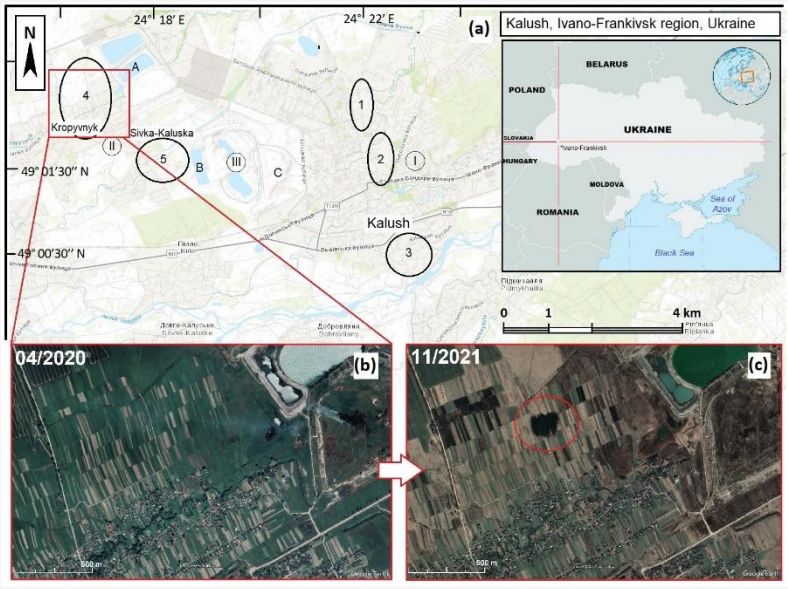

Figure 1: (a) Kalush-Holyn deposit: I – mine „Kalush", 1 – Northern kainite field, 2 – Central kainite field, 3 – Khotin sylvinite field; II – Novo-Holyn mine, 4 – Eastern Holyn, 5 – Sivka-Kaluska; III – flooded Dombrovskyi quarry, A – tailings ponds, B – collector tanks, C – quarry dumps; Satellite photo of the area of Kropyvnyk village (b) before, and (c) after lake formation in the sinkhole zone

1.2 Conducted Research

The monitoring of the current state of geodynamic activity in the territories of the Kalush-Holyn deposit, particularly in the area of Kropyvnyk village, is conducted based on the complex geophysical, geochemical, and geodetic methods. The detailed results of the geophysical monitoring in the Kalush-Holyn deposit are presented in the research paper [21]. The obtained results confirmed the effectiveness of using the method of the Earth's natural pulsed electromagnetic field for predicting the development of collapse-subsidence processes. The interpretation of gravimetric data allowed for determining the position of decompression zones and tracking their evolution over time. A clear correlation has been established between the geophysical data and geodetic observations.

The actual changes in terrain topography over the mining fields are defined by geodetic observations performed by the geometric levelling method. The high-precision differential levelling in the Kalush-Holyn deposit began in 1965. These studies were conducted systematically until 2010. In 2013, the city of Kalush, and the villages of Kropyvnyk and Sivka-Kaluska were declared as zone of emergency ecologic situation. After a several-year pause, the studies were resumed. Additionally, archival data on differential levelling for the period 1968-2010 were systematized [22]. In 2021, systematic geodetic observations began in the sinkhole area formed in Kropyvnyk village, with high-precision levelling conducted annually.

In recent years, the results of satellite synthetic aperture radar (SAR) monitoring have increasingly been used to analyze the territory of the Kalush-Holyn deposit. The growing use of satellite radar data has led to the widespread application of the SAR interferometry method (InSAR) in areas affected by anthropogenic activity, particularly in underground mining regions [23]. This is due to the versatility of the survey results, which can be utilized both for creating digital terrain models [24] and [25] as well as for determining Earth's surface deformations caused by natural [26] and anthropogenic factors [27]. Besides, the SAR results of certain satellite missions are freely available. And in recent years, an archive of images with high spatial-temporal resolution has been formed. In combination with the ground-based geodetic methods, the data from satellite radar surveying enable the creation of reliable maps of the Earth's surface deformation rates for the areas of mining complexes [10] [28] and [29]. There are various methods and approaches for the time series processing of radar images. The most common among them include the Small Baseline Subset method (SBAS) [11] and the Persistent Scatterer method (PSI) [30][31] and [32], and also the combination of these methods.

For the first time, the InSAR method was applied to the Kalush-Holyn deposit area using Sentinel-1 satellite data from 2016 to 2017 [33] and [34]. Then, the highest deformation velocities were detected over the mining field "Khotin" (mine "Kalush"). The average subsidence rates were within the range of 5-20 mm/year. The processing of the time series of SAR images was performed using the PSI and SBAS methods. This research was further developed in the work [35]. The InSAR method was applied for the territories of the "Kalush" mine, which are mostly concentrated in urban areas. 36 SAR images of the Sentinel-1 satellite were used for research, covering the period from mid-2018 to late 2022. It was found that the maximum value of the deformation rate decreased in comparison with the previous research period of 2016-2017 [33], from 20 mm/year to 4 mm/year. This points to a decreasing trend in subsidence in this area. The SAR data were processed by the PSI method.

Dominant scatterers of radar signals are mainly concentrated on artificial structures and objects (houses, roads, etc.). Therefore, the PSI method is especially effective for deformation analysis in urbanized areas. In areas where vegetation predominates and artificial structures are absent, the PSI method yields unreliable results. This is explained by the decorrelation of a signal on different time images, which appears owing to plant vegetation, snow accumulation, and so on. Decorrelation can be overcome by reducing a temporal baseline. The SBAS method is based on the principle of using interferograms obtained from images with a short temporal baseline. This method demonstrates highly effective results in areas where scattered signals from satellite's radar dominate, such as arable land, undeveloped regions, and similar environments.

Small Baseline Subset InSAR (SBAS-InSAR) has been extensively applied for monitoring surface deformation in mining areas, offering the ability to reconstruct both residual and active ground movements. Despite its widespread use, SBAS-InSAR results can be affected by spatial and temporal decorrelation, atmospheric delays, and data quality, which has motivated the integration of levelling measurements as constraints to correct subsidence estimates and improve accuracy to within ±50 mm/year [36]. In addition, combining SBAS-InSAR with archival radar data allows reconstruction of early-stage surface displacement and deformation rates in underground mining collapse areas, enabling identification of long-term stable settlement patterns, sudden deformation events, and high-risk zones, thus

supporting reliable forecasting and territorial safety management [37]. Further advances include the integration of SBAS-InSAR with UAV photogrammetry, which enhances precision by resolving line-of-sight inconsistencies and mitigating coherence and measurement errors, while facilitating accurate subsidence prediction using neural network models [38] and [39]. Importantly, SBAS-InSAR has also proven effective for post-mining environments, capturing residual subsidence and uplift over decommissioned underground mines, reflecting both past mining activity and groundwater recharge processes [40]. Collectively, these studies highlight the versatility and growing methodological sophistication of SBAS-InSAR for comprehensive deformation monitoring and prediction in complex mining contexts.

Figure 2 shows that the development of deformation processes in the area of Kropyvnyk village (formation of a sinkhole and its subsequent flooding) occurs generally in a non-urbanized area characterized by dense vegetation cover, where the application of PSI method is limited due to the loss of signal coherence. Therefore, to ensure reliable radar monitoring results, the SBAS method was applied. The scientific novelty of the obtained results lies in confirming the effectiveness of the SBAS method under conditions of intensive temporal decorrelation caused by vegetation dynamics, seasonal surface changes, and rapid vertical displacements. The use of time series of interferograms with short temporal baselines made it possible to preserve the coherence of the distributed radar signal and to obtain reliable estimates of deformation velocities. Thereby expanding the practical capabilities of satellite radar monitoring for the territories located above underground mining areas.

2. Data and Method

Depending on the ultimate purpose of using the SAR data, there are several options for accessing satellite monitoring results. Typically, C- and L-band SAR images (medium resolution) are freely available. In contrast, X-band images (with a resolution of 3×3 m) and other high and ultra-high-resolution images (up to 0.25 m) are distributed either on a commercial basis or upon request for specific scientific research. Nevertheless, as practical experience shows, medium-resolution images can be an effective tool for solving a wide range of geospatial tasks, including subsidence studies in mining fields.

The Sentinel-1 satellite mission is one of the primary sources of C-band SAR data. Given the need to process large time series of images for monitoring long-term geodynamic processes, the input data were downloaded using the services of the Alaska Satellite Facility Distributed Active Archive Center (https://asf.alaska.edu/). Processing large time series of SAR data has several important features that must be considered to optimize the research process and achieve reliable results. Let us explore the key aspects related to data processing: 1. *Data volume and system resources for processing*. The memory capacity occupied by one radar image varies from 4 to 8 GB. Therefore, processing large time series of images, which can number in the tens or even hundreds, requires not only substantial computing resources but also the ability to store large volumes of data locally. 2. *Automation of time series processing algorithms*. Given the large number of images and the need to perform repetitive operations, modern data processing approaches require automated algorithms. Automation is crucial in the initial stages, which include applying orbit files, subsetting the area of interest, co-registration of images, and interferogram formation. A well-known example of an automated algorithm is SNAP2StaMPS [41], which is used to prepare data for processing by the PSI method 3. *Updating of software packages*. Due to the rapid development of the industry and the continuous accumulation of archival data, there is often a need to reconfigure processing parameters after updates to data libraries and software. Similar challenges arise from transitions to new platforms (e.g., from Open Access Hub to Copernicus Browser) and updates to existing services that distribute SAR data, such as the planned transfer of ASF site content to a new domain by 2026.

The large time series processing of SAR data is a complicated procedure that requires considering the above-listed factors to optimize work with vast scopes of information. For this purpose, the given article uses the data prepared by the automated data processing platform in ASF's cloud servers. The service On-Demand Processing was developed and implemented by ASF to maximize the processing rate, excluding the need to download large volumes of data and focus on the analysis of monitoring results [29]. The Sentinel-1 satellite data were used to study the development of deformation processes in the vicinity of Kropyvnyk village. Time-series analysis was performed using the NSBAS (New Small Baseline Subset) inversion approach implemented in MintPy (Miami Insar time-series software in Python) [42]. Unlike the original SBAS algorithm proposed by [43], the NSBAS method introduces temporal smoothing constraints, improving the stability of the inversion in the presence of an incomplete interferogram network

[44]. For each interferogram k, the observed unwrapped phase ϕ_k is expressed in Equation 1 [43]:

$$\phi_k = \frac{4\pi}{\lambda}\left[u(t_i) - u(t_j)\right] + \phi_k^{atm} + \phi_k^{noise}$$

Equation 1

Where: λ – radar wavelength, $u(t_i)$, $u(t_j)$ – cumulative displacement at acquisition times t_i and t_j, ϕ_k^{atm} – atmospheric delay contribution, ϕ_k^{noise} – decorrelation and measurement noise. After atmospheric correction and filtering, the deformation component is isolated for time-series inversion.

The classical SBAS linear system formulation is written as Equation 2 [43]:

$$Gm = d$$

Equation 2

Where m is the vector of unknown cumulative displacements at acquisition dates, d is the vector of observed interferometric phases converted to LOS displacement, G is the design matrix describing temporal differences between acquisition pairs. The design matrix G contains −1 and +1 entries corresponding to master and slave acquisition dates, respectively, forming a temporal difference operator [45]. Because one acquisition is chosen as reference ($d(t_0)$=0), the system is rank-deficient and typically solved using Singular Value Decomposition or least squares. The NSBAS approach introduces temporal smoothing constraints to improve solution stability, especially in the presence of disconnected interferogram networks. The regularized system takes the form shown in Equation 3:

$$\begin{bmatrix} G \\ \alpha R \end{bmatrix} m = \begin{bmatrix} d \\ 0 \end{bmatrix}$$

Equation 3

Where R is the temporal smoothing operator, α is the regularization parameter. A common form of R enforces smooth temporal evolution via second-order finite differences:

$$Rm = \left[u_{t+1} - 2u_t + u_{t-1}\right]$$

Equation 4

This minimizes unrealistic acceleration in the displacement time series. The solution is obtained by minimizing the cost function (Equation 5):

$$\min_m = (\| Gm - d \|^2 + \alpha^2 \| Rm \|^2)$$

Equation 5

Which corresponds to Tikhonov regularization [46]. Assuming approximately linear deformation over time, velocity v is estimated from the cumulative displacement time series using least squares regression (Equation 6):

$$u(t) = vt + c$$

Equation 6

Where v denotes the mean LOS velocity and c is a constant offset. In vector form, the velocity parameter is estimated as in Equation 7:

$$v = (\mathbf{t}^T\mathbf{t})^{-1}\mathbf{t}^T\mathbf{u}$$

Equation 7

Where $\mathbf{t}$ is the vector of acquisition times and $\boldsymbol{u}$ is the vector of cumulative displacements.

This regression is applied independently to each pixel in order to generate the mean velocity map. The preliminary preparation of interferograms was performed via the automated platform HyP3 (Hybrid Pluggable Processing Pipeline). Downloading of Hyp3 data and analyzing time series through MintPy tools were performed in the Jupyter Notebook environment. Jupyter Notebook is an interactive environment for writing and executing code directly in a web browser. Its main feature is the ability to combine code, text, visualizations, and explanations in a single document, thus making it an efficient and convenient environment for working with SAR data. Access to the Jupyter Notebook environment is provided by the OpenSARlab online platform. The flow chart of the data processing chain is presented in Figure 2.

Figure 2 shows that the processing methodology consists of two main steps, which are firstly realized via the web interface of the ASF archive center, and then in the interactive Jupyter Notebook environment.

Step 1: On-demand Processing using the Automated HyP3 Platform

The first preparatory stage of processing was performed using the ASF's service Vertex. For this, a request was made for automated data processing by the Hyp3 platform. HyP3 (Hybrid Pluggable Processing Pipeline) is a free-of-charge cloud-based online platform for processing radar data from Sentinel-1 satellite. It was developed by NASA and is currently being implemented based on the archive center Alaska Satellite Facility [47].

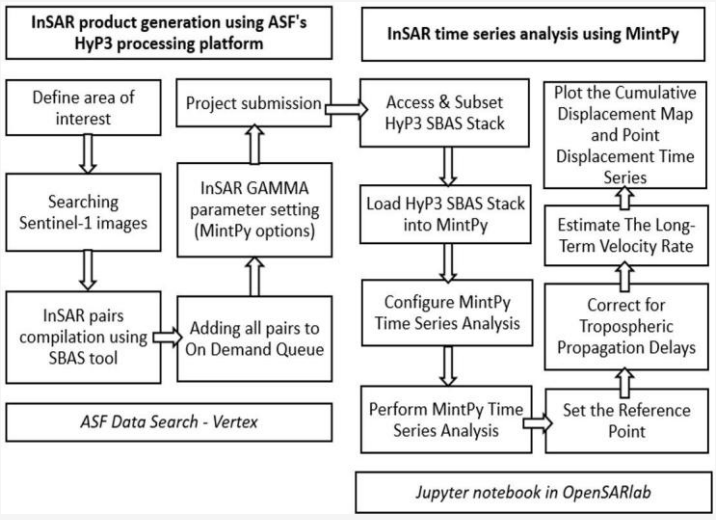

Figure 2: The processing chain of satellite SAR data using the NSBAS method with the MintPy software package

By sending their requests, users can quickly get pre-processed data in the cloud environment (wrapped or unwrapped differential interferograms). This saves time and local resources, avoiding the need to download and process any raw SAR data. The area of interest was focused on the Kalush-Holyn field. A suitable SAR image was selected, which was acquired by the Sentinel-1 satellite from an ascending orbit. Then, using the SBAS tool of Vertex service, the pairs of images were chosen to be used for forming interferograms. The following parameters served as input data for data selection: research period April 04, 2021 – March 19, 2024; the maximum value of perpendicular baseline was 200 m; the maximum temporal baseline was 36 days. As a result, 295 interferometric pairs were formed. When creating a request to process the data selected, the InSAR GAMMA processor was chosen. The parameters, required for further processing in MintPy, were established (set MintPy options).

Step 2: Time-series Analysis of SAR Data Using MintPy

MintPy (Miami INsar time-series software in Python) is an open-code software package (https://mintpy. readthedocs.io/en/latest/) for analyzing time-series of satellite radar interferometry data. It supports the data sets formed in various formats: ISCE, ARIA, FRInGE, HyP3, GMTSAR, SNAP, GAMMA, and ROI PAC. Due to processing, one can get the spatio-temporal displacements of the Earth's surface towards the satellite's line of sight (LOS). This package may be known by users as PySAR (up to version 1.1.1). For versions 1.1.2 and the latest, the name MintPy is used. The algorithm of MintPy software package is realized in the Jupyter Notebook environment. It is a convenient tool that provides step-by-step running of scripts, configuring of variable parameters, and selection of data visualization options. Along with the code and its output, the Jupyter Notebook includes text fields that describe the executed processes, the algorithm of required operations, and explanatory notes. The whole concept is aimed at maximally simplifying the process of analyzing the data time series. Typically, the process of awaiting the dataset processing results using the HyP3 platform does not exceed 24 hours. Transferring data from HyP3 platform to the project work folder in Jupyter Notebook is the most time-consuming process (up to a few hours). The HyP3 dataset is downloaded into MintPy only once. After that, the work with data may be repeated with different settings of analysis parameters.

To ensure the reliability of the interferometric phase observations used in the time-series analysis, a coherence threshold of 0.6 was applied prior to the NSBAS inversion. Interferometric coherence represents the degree of phase correlation between two SAR acquisitions and ranges from 0 (complete decorrelation) to 1 (perfect phase stability). Low-coherence measurements are more strongly affected by decorrelation noise, which can propagate into the least-squares inversion and degrade the stability of the reconstructed deformation time series. The selected threshold of 0.6 provides a compromise between phase quality and spatial coverage. As illustrated in Figure 3, which presents the interferogram network colored by average spatial coherence, the majority of interferometric pairs exhibit coherence values equal to or greater than 0.6.

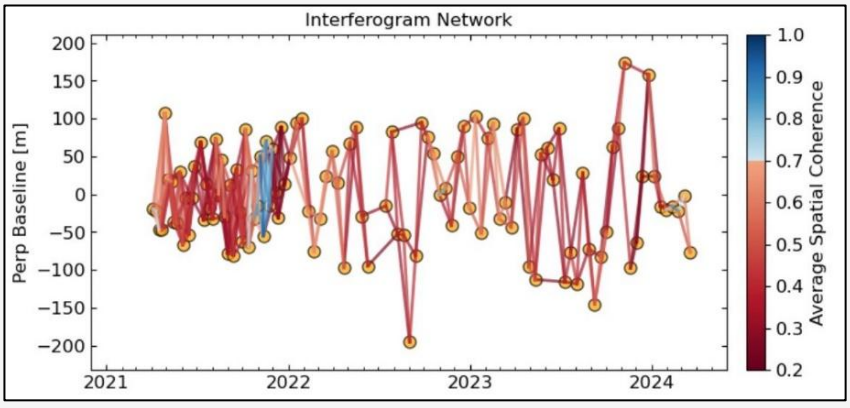

Figure 3: Interferogram network colored by average spatial coherence

This indicates generally stable phase behavior within the dataset and supports the suitability of the chosen threshold.

During the analysis of the time series in MintPy, a reference point is selected. The selection of a reference point makes it possible to bind a set of interferograms to a single (reference) pixel. By default, the MintPy automatically selects a pixel with the highest coherence value. A reference point is considered a stable area in the image and can be specified by its coordinates. Such a point can be represented by the position of GNSS station with the known speed of spatial movements, which is available in the image. During the study period (2021-2024), the permanent station located near the Kalush-Holyn field was not yet in operation. It was erected in early 2025. Therefore, the MintPy algorithm automatically selected the most stable reference point.

Applying corrections for tropospheric propagation delays is an optional step. However, it is worth mentioning that tropospheric signal delay has the greatest impact on the results of SAR monitoring [48]. Thus, to achieve reliable research results, the correction of atmospheric impact was introduced. The MintPy provides an effective determination of tropospheric signal delay based on the data from up-to-date climate models ERA5 [49]. These models are developed by the European Center for Medium-Range Weather Forecasts (ECMWF) and are publicly available via the CDS (Climate Date Store) service. The deformation rate obtained from InSAR time-series analysis is a general assessment of surface movement towards the satellite's LOS. This velocity determines the generalized deformation trend for the entire period of research. The results are supplemented by a linear model of data approximation of time series for each pixel on the created map. The Cumulative Displacement Map represents the development of the deformation process over time. Owing to the use of a time scale, one can follow the development of the subsidence process at a certain point in time. The point-click on the map displays a time series of surface movement at the selected point.

3. Results and Validation

The formation of a sinkhole in the area of Kropyvnyk village, which is located above the area of mine "Novo-Holyn", started in 2018. The threatening consequences of subsidence of the Earth's surface, which were visually seen in 2021, became the reason for the prompt implementation of comprehensive monitoring of the territory. The deformation processes are caused by the barrier pillar failure between the mine cavities. Meanwhile, subsidence troughs of different sizes and localization are gradually forming. It is important to note, that the obtained results enable us to track not only the visually seen deformations in the form of sinkholes or ponds. The radar monitoring results allow us to identify the areas where deformation processes are just about to start developing.

A map of the average deformation rates of the Kalush-Holyn deposit for the entire research period was produced based on the NSBAS method data processing results. The rates presented on this map are defined towards the satellite's line of sight (LOS). The obtained map of velocities shows a generalized assessment of deformation processes in the mining field "Novo-Holyn". The map clearly shows two areas (marked by red circles in Figure 4) with velocity values exceeding 5 cm/year: Zone 1 - an area to the North of Kropyvnyk village in the region of the formed sinkhole, flooded with water; Zone 2 - the roof of a reclaimed tailings pond.

Figure 4 highlights Zone 3, which requires additional attention. The deformation zone is gradually extending southeast of Zone 1. It is the area within the residential space of the urban settlement, where major subsidence of the Earth's surface is also observed. The subsidence rates in Zone 3 are

significantly lower than those in Zone 1, still, the situation poses a danger for residents and needs urgent administrators' decisions. The MintPy software package enables the analysis of deformation development in the given area at different points in time. To accomplish this, cumulative deformation maps, time-series plots, and corresponding velocity trends are employed. Figure 5 presents time-series plots for areas exhibiting the highest deformation rates in the vicinity of residential buildings (Zone 1) and in Kropyvnyk village (Zone 3). The plots show the development of subsidence in the mining field "Novo-Holyn" since April 2021. The deformations are indicated in centimeters and reflect the movement of the Earth's surface along the satellite's LOS (positive values - lifting; negative values - subsiding).

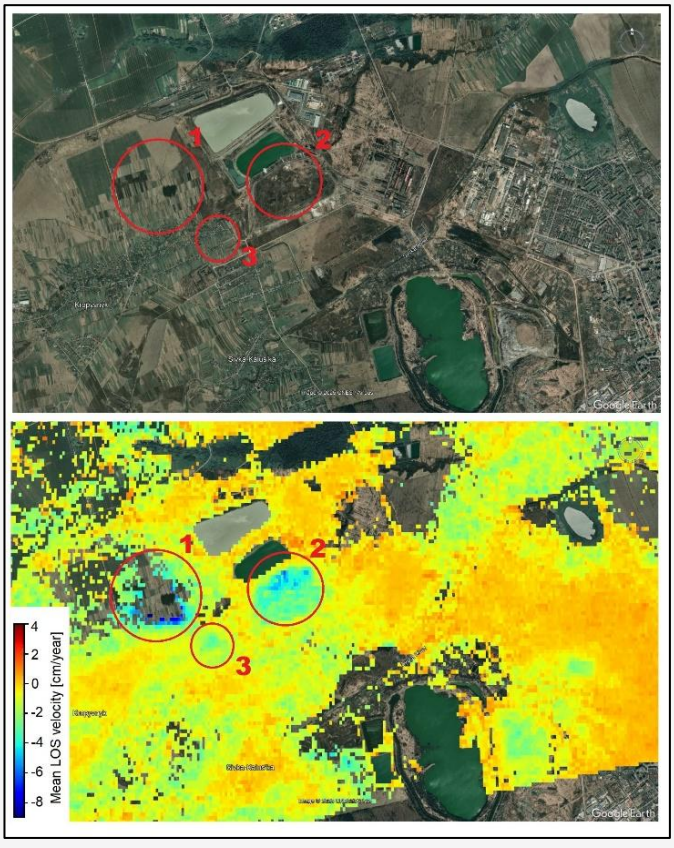

Figure 4: Satellite image of the Kalush-Holyn deposit and a map of average deformation velocities of the Earth's surface for the period 04.04.2021-19.03.2024

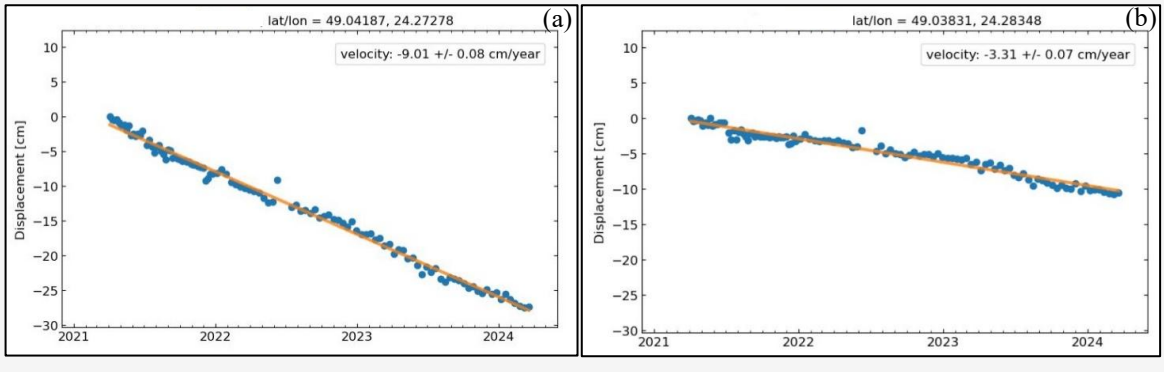

Figure 5: Time-series plots showing the temporal evolution of subsidence with highest deformation rates and the linear trend of deformation in the Novo-Holyn mining field during the period 04.04.2021-19.03.2024 (a) zone 1, and (b) zone 3

Analysis of the deformation time-series plots enables the estimation of subsidence rates and the derivation of quantitative indicators for forecasting purposes. The deformation map derived from radar satellite observations indicates that deformation rates near the residential development of the settlement reach up to 9 cm/year. The root mean square error of the estimated deformation rates does not exceed 1 cm. The results of satellite radar monitoring require verification. One of the most common ways to confirm the InSAR results is by comparing them with ground-based geodetic measurements. Four campaigns (2021-2024) of geodetic observations were conducted at the research area to monitor the vertical displacements of benchmarks of the levelling network. The levelling procedure was carried out using the methodology of second-order high-precision differential levelling. The levelling network was established during the deposit extraction phase to monitor Earth's surface deformations over the mining fields. The interval between the benchmarks varies across different levelling lines, with distances of 20 m, 25 m, or 50 m. Based on the differences in the benchmark's measured elevations for each campaign, the rate of vertical movements of benchmarks was calculated for four levelling lines: 111-16, 134-4, 1-21, and 9-11 (Figure 6).

Figure 6: The levelling scheme over the Novo-Holyn mining field and the number of end-line benchmarks

The MintPy software package includes an easy-to-use tool for comparing InSAR monitoring results with differential levelling data – the Plotting Motion Transect. After selecting two points on the velocity map, we obtain a graph of deformation velocities along the profile line. The profile line's position exactly corresponds to the location of the levelling line on the landscape, as the benchmarks are arranged in a straight line. Since the SAR monitoring results represent deformation velocities along the satellite's LOS, comparing them with differential levelling requires calculating the vertical component of the deformation vector. To do this, the Equation 8 was used [50]:

$$V_{vert} = \frac{V_{LOS}}{\cos\theta}$$

Equation 8

Where V_{vert} is the vertical component of deformation velocity; V_{LOS} is the deformation velocity along the satellite's LOS; θ is the radar incidence angle.

Figure 7 presents a comparison of vertical deformation rates obtained from SAR monitoring results by the Sentinel-1 satellite and high-precision differential levelling data along four profile lines.

Profile 111-16: This line passes to the north of the lake formed in the sinkhole zone. The levelling results indicate deformation velocities reaching up to -41.3 cm/year. The maximum subsidence rate, according to the InSAR results, is -13.1 cm/year. Both methods demonstrate a high level of agreement regarding the position of the subsidence trough. However, in terms of quantitative measurements, the InSAR method significantly underestimates the rapid deformations at the center of the sinkhole.

Profile 134-4: It crosses the central part of the subsidence trough. The gaps in the levelling results graph are due to the flooding of benchmarks in the central part of the funnel. The maximum recorded velocities reach -47.2 cm/year. The remaining gaps in the graph correspond to benchmarks that are either lost or not found. Similar to the previous profile, the InSAR and levelling results show excellent agreement for deformation velocities up to 10-15 cm/year. The maximum deformation rates obtained from the InSAR results are 12-13 cm/year. The spike of -10 cm/year in the graph (400 meters from benchmark № 134) is due to errors in the results, as a lake was formed in this location.

Profile 1-21: This line characterizes the deformations that are actively increasing in Zone 3 (see Figure 4). The profile line passes along the residential area of the urban settlement. The results from both methods indicate the same subsidence trend, with the maximum values observed at benchmark № 21. On average, the difference in deformation velocities between the two methods does not exceed 1 cm/year.

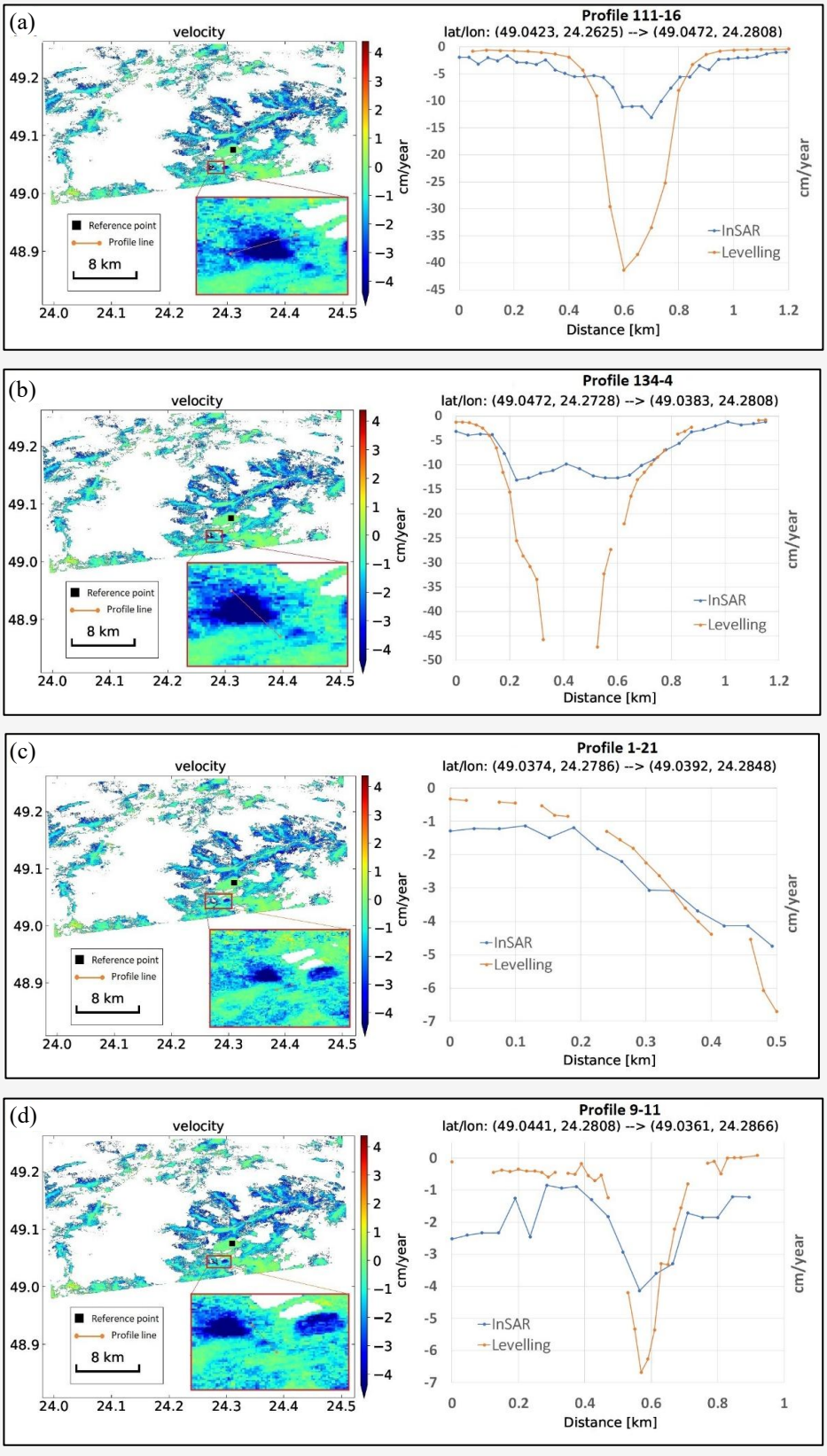

Figure 7: Graphs of vertical velocities of Earth's surface deformations based on the results of InSAR and high-precision levelling along the profile lines: (a) 11-16, (b) 134-4, (c) 1-21, and (d) 9-11

However, this difference increases to 2 cm/year at the end of the profile line. We believe this is due to the rapid subsidence of the last two levelling marks, which are spaced 20 meters apart. Considering the resolution of Sentinel-1 satellite images, these two levelling marks may fall within the range of 1-2 pixels. Consequently, the resulting deformation velocity map captures such localized deformations with lower precision.

Profile 9-11 is located perpendicularly to line 1-21 and also describes the deformation processes in Zone 3 (Figure 4). The gaps in the levelling graph are due to the absence or loss of corresponding benchmarks. In the central part of the graph (500-550 m along the profile), the lack of benchmark data is effectively supplemented by the InSAR results. However, the data differ significantly at the beginning of the profile (0-300 m) because this area is located in a wetland. During levelling, some of the benchmarks are submerged, while others are not found. Such terrain conditions significantly affect signal coherence, which, in turn, reduces the reliability of the InSAR monitoring results. The correlation between velocity data obtained from the deformation map and second-class levelling data was calculated. The correlation coefficients for each profile line are as follows: r = 0.76 (profile 111-16), r = 0.62 (profile 134-4), r = 0.93 (profile 1-21), and r = 0.74 (profile 9-11). All values are statistically significant.

4. Discussion

The obtained research results are influenced by three factors: the specific conditions of the studied object, the parameters of the input data, and the characteristics of their processing. The specific conditions of the studied object involve rapid subsidence of the Earth's surface, with values reaching up to 50 cm/year. Additionally, localized subsidence is observed over an area spanning several tens of square meters. In such cases, discrepancies between the levelling and InSAR results arise due to theoretical limitations in determining deformation velocities using SAR monitoring data. It is known that, under the assumption of a linear deformation model, the maximum deformation rate detectable by the InSAR method depends on the radar wavelength and the temporal baseline between acquisitions [50]. The wavelength of the radar signal for the Sentinel-1 satellite is 5.6 cm, while the time interval between observations is 12 days. Based on these parameters, the InSAR method is capable of detecting deformation velocities of up to 42.6 cm/year. Figures 7(a) and 7(b) show that the actual deformation velocities are either close to the theoretically possible values or exceed them. Therefore, in the funnel formation zone, where subsidence velocities increase abruptly, the resulting values differ significantly.

In addition, sensor parameters influence not only the radar wavelength but also the spatial resolution of the imagery. For the Sentinel-1 satellite, the resolution is 5 × 14 m. This affects the sensitivity of the method under conditions of rapid and localized subsidence, where deformations may correspond to only a few pixels within the image.

When processing the data using the HyP3 platform, the number of looks was set to 10×2. This means that the results are averaged over 10 pixels in the range direction and 2 pixels in the azimuth direction. As a result, this reduces the method's sensitivity to local deformations covering small areas. The comparison of the InSAR and levelling results in Figures 7(c) and 7(d) illustrates this point. The local subsidence rates of some levelling benchmarks, spaced 20 meters apart, are determined by the InSAR method with lower reliability. Another factor that affects the discrepancy between the results of differential levelling and InSAR, to some extent, is the incomplete synchronization of results in time. The graphs present the results of radar survey processing for the period 04.04.2021-19.03.2024. The levelling campaigns were carried out in August of each year. Thus, in 2024, there is a 5-month gap between March 2024 (the latest SAR image) and August 2024 (the latest levelling campaign). During these 5 months, some benchmarks could have significantly changed their vertical position. As a result, the InSAR results show lower velocity values.

5. Conclusions

The studies presented in this paper led to several conclusions regarding approaches to processing and analyzing satellite SAR monitoring results:

1. The use of automated interferogram preparation on cloud servers via the HyP3 platform is an effective and modern approach for processing large time series of SAR images. This method significantly reduces the consumption of local system resources and allows for a much faster analysis of the obtained data.

2. The presented workflow demonstrates that the SBAS-based InSAR time-series analysis can remain effective even under conditions of intensive temporal decorrelation caused by vegetation dynamics, seasonal surface changes, and rapid vertical displacements typical for mining regions. The use of interferogram networks with short temporal baselines, combined with coherence-based filtering and NSBAS inversion, makes it possible to preserve the stability of the distributed

radar signal and obtain reliable deformation velocity estimates. This methodological approach can be generalized and applied to other territories affected by underground mining or similar geodynamic processes, thereby expanding the practical capabilities of satellite radar monitoring for areas where conventional interferometric techniques are often limited by decorrelation effects.

3. Maps of average surface deformation velocities obtained by the NSBAS method for the Kalush-Holyn potash salt deposit closely correspond with previous geophysical studies and geodetic observations carried out using the differential levelling method. Given the high frequency of satellite acquisition over the study area (every 12 days), the InSAR method provides reliable tracking of the progression of deformation processes. We believe that the InSAR method should serve as an intermediate stage in a comprehensive study of the region's geodynamics, as it allows for the localization of areas where deformation processes begin to develop, which may not be detected based on forecast data from geophysical methods. In addition, ground-based geodetic methods (high-precision levelling, GNSS) serve to verify SAR monitoring results and accurately determine the amplitude of surface motions.

4. The results of radar monitoring align with high-precision levelling in areas where deformation rates remain below the theoretical limits that can be detected using C-band SAR images acquired by the Sentinel-1 satellite. However, in regions where deformation rates approach or exceed 42.6 cm/year, the InSAR method does not yield reliable results.

Acknowledgment

We are totally grateful for the granted access to the OpenSARLab deployment by ASF Distributed Active Archive Center. The Synthetic Aperture Radar (SAR) workflow using MintPy was implemented via the JupyterHub computing environment. The input data were processed by the HyP3 online platform, which was also developed and operated by the Alaska Satellite Facility (ASF).

References

[1] Li, S. Y., Zhao, J. Y., Li, J. Q., Li, M. J., Wang, H. G. and Guo, H. P., (2024). Numerical Simulation of Ground Subsidence Due to Oil and Gas Extraction from Creeping Reservoirs. *58th U.S. Rock Mechanics/Geomechanics Symposium*, https://doi.org/10.56952/ARMA-2024-0963.

[2] Severi, P., Mazzoni, R. and Martelli, L., (2021). Oil and Gas Activities in Emilia-Romagna Region (Italy): Land Deformation and Territory Protection. *Bollettino Di Geofisica Teorica Ed Applicata*, Vol. 62(2). https://doi.org/10.4430/bgta0327.

[3] Yang, C., Zhang, D., Zhao, C., Han, B., Sun, R., Du, J. and Chen, L., (2019). Ground Deformation Revealed by Sentinel-1 MSBAS-InSAR Time-Series over Karamay Oilfield, China. *Remote Sensing*, Vol. 11(17). https://doi.org/10.3390/rs11172027.

[4] Chen, M., Tomás, R., Li, Z., Motagh, M., Li, T., Hu, L., Gong, H., Li, X., Yu, J. and Gong, X., (2016). Imaging Land Subsidence Induced by Groundwater Extraction in Beijing (China) Using Satellite Radar Interferometry. *Remote Sensing*, Vol. 8(6). https://doi.org/10.3390/rs8060468.

[5] Chaussard, E., Milillo, P., Bürgmann, R., Perissin, D., Fielding, E. J. and Baker, B., (2017). Remote Sensing of Ground Deformation for Monitoring Groundwater Management Practices: Application to the Santa Clara Valley During the 2012–2015 California Drought. *Journal of Geophysical Research: Solid Earth*, Vol. 122(10); 8566–8582. https://doi.org/10.1002/2017JB014676.

[6] Botey I Bassols, J., Vàzquez-Suñé, E., Crosetto, M., Barra, A. and Gerard, P., (2021). D-InSAR Monitoring of Ground Deformation Related to the Dewatering of Construction Sites. A Case Study of Glòries Square, Barcelona. *Engineering Geology*, Vol. 286. https://doi.org/10.1016/j.enggeo.2021.106041.

[7] Gezgin, C., (2022). The Influence of Groundwater Levels on Land Subsidence in Karaman (Turkey) Using the PS-InSAR Technique. *Advances in Space Research*, Vol. 70(11); 3568–3581. https://doi.org/10.1016/j.asr.2022.08.003.

[8] Marghany, M., (2021). *Advanced Algorithms for Mineral and Hydrocarbon Exploration Using Synthetic Aperture Radar*. Elsevier. https://doi.org/10.1016/C2019-0-04105-2.

[9] Fazilova, D., Makhmudov, M., and Magdiev, K. (2023). Analysis of Crustal Movements in the Angren-Almalyk Mining Industrial Area Using GNSS Data. *International Journal of Geoinformatics*, Vol. 19(11), 12–19. https://doi.org/10.52939/ijg.v19i11.2915..

[10] Wang, L., Yang, L., Wang, W., Chen, B. and Sun, X., (2021). Monitoring Mining Activities Using Sentinel-1A InSAR Coherence in Open-Pit Coal Mines. *Remote Sensing*, Vol. 13(21). https://doi.org/10.3390/rs13214485.

[11] Xu, Y., Li, T., Tang, X., Zhang, X., Fan, H. and Wang, Y., (2022). Research on the Applicability of DInSAR, Stacking-InSAR and SBAS-InSAR for Mining Region Subsidence Detection in the Datong Coalfield. *Remote Sensing*, Vol. 14(14). https://doi.org/10.3390/rs14143314.

[12] Hlotov, V. and Biala, M., (2022). Spatial-Temporal Geodynamics Monitoring of Land Use and Land Cover Changes in Stebnyk, Ukraine Based on Earth Remote Sensing Data. *Geodynamics*, Vol. 1(32); 5–15. https://doi.org/10.23939/jgd2022.02.005.

[13] Khevpa, Z., Dolin, V., Yakovlev, E., Kuzmenko, E. and Bagriy, S., (2022). Development of a Water and Ecological Emergency from Mine Flooding of Stebnyk Potassium Deposit Owing to Natural and Technogenic Factors. *Geochemistry of Technogenesis*, Vol. 35; 51–56. https://doi.org/10.32782/geotech2022.35.09.

[14] Pakshyn, M., Lyaska, I., Kablak, N. and Yaremko, H., (2021). Study of the Influence of Mining Products from the Mines of the Solotvyn Salt Mine on the Earth's Surface, Buildings and Structures Using Satellite Radar Monitoring. *Geodynamics,* Vol. 2(31); 41–52. https://doi.org/10.23939/jgd2021.02.041.

[15] Kablak, N., Pukanska, K., Bartoš, K., Savchyn, I., Nychvyd, M., Kalynych, I., Fehér, J. and Prodanets, I., (2024). Application of Integrated Geodetic and UAV Technologies for Monitoring Environmental Changes Due to the Mining Activities in Solotvyno Salt Mine, Ukraine. *Acta Montanistica Slovaca*, Vol. 29(2); 267–275. https://doi.org/10.46544/AMS.v29i2.03.

[16] Savchuk, S., Kablak, N., Kalynych, I. and Nychvyd, M., (2023). Application of InSAR Technology for Monitoring Geodynamic Processes (A Case Study of the Solotvyn Salt Mine). *Geophysics and Geodynamics: Prediction and Monitoring of Geological Medium*, 10–12 October 2023. Lviv, Ukraine. (in Ukrainian)

[17] Gera, O., Hrynishak, M. and Dorosh, L., (2021). Factors of the Subsidence trough Formation over the Underground Mine Workings. *Technical Sciences and Technologies*, Vol. 2(24); 227-234. https://doi.org/10.25140/2411-5363-2021-2(24)-227-234.

[18] Anikeyev, S. G., Kuzmenko, E. D., Bagriy, S. M., Hablovskyi, B. B. and Dzoba, U. O., (2019). The Results of Gravimetric Monitoring on the Worked-out Potassium Salt Deposit in the Precarpathian Region. *Monitoring 2019*, 1–5. https://doi.org/10.3997/2214-4609.201903167.

[19] Golovchak, V., (2012). Kalusko-Holinskoye Deposit of Potash Salts. Encyclopedia of Modern Ukraine. NAS of Ukraine, Scientific Research School. Kyiv: Institute of Encyclopedic Research of NAS of Ukraine. https://esu.com.ua/article-10695.

[20] Golovchak, V., (2010). The State of Mining and Industrial Geocomplexes of the Kalush-Golinsky Deposit of Potash Salts and Measures for their Ecological Optimization. *Ecological Safety and Balanced Resource Use*, Vol. 2; 4–13.

[21] Bagriy, S., Kuzmenko, E. and Dzoba, U., (2020). Correlation of Natural Pulsed Electromagnetic Field of the Earth with Stresses and Deformations, which Appeared in Exhausted Salt Fields in the Precarpathians Forkarst Creation Forecasting. *Visnyk of Taras Shevchenko National University of Kyiv. Geology,* Vol. 2(89); 79-88. http://doi.org/10.17721/1728-2713.89.11.

[22] Burak, K., Kuzmenko, E., Bahriy, S., Hrynishak, M., Melnychenko, G., Mykhailyshyn, V., Kovtun V. (2014). Peculiarities of Geodetic Monitoring and Forecasting of Geotechnogenic Dynamics in Mining Fields of Potash Deposits. *Bulletin of Geodesy and Cartography,* Vol. 5(92); 12–18. (in Ukrainian).

[23] Colombo, D. and MacDonald, B., (2015). Using Advanced InSAR Techniques as a Remote Tool for Mine Site Monitoring. *Slope Stability*. [Online]. Available: https://site.tre-altamira.com/wp-content/uploads/2015_InSAR_mine-site_monitoring.pdf. [Accessed: Apr. 6, 2026].

[24] Marghany, M., (2013). DInSAR Technique for Three-Dimensional Coastal Spit Simulation from Radarsat-1 Fine Mode Data. *Acta Geophysica*, Vol. 61(2); 478–493. https://doi.org/10.2478/s11600-012-0061-5.

[25] Aziz, M., Pa'suya, M., Talib, N., Din, A., Hashim, S., and Ramli, M. (2023). Vertical Accuracy Assessment of Improvised Global Digital Elevation Models (MERIT, NASADEM, EarthEnv) Using GNSS and Airborne IFSAR DEM. *International Journal of Geoinformatics*, Vol. 19(12), 65–82. https://doi.org/10.52939/ijg.v19i12.2979.

[26] Tretyak, K. R. and Kukhtar, D. V., (2023). Application of Sentinel-1 Radar Interferometric Images for the Monitoring of Vertical Displacements of the Earth's Surface Affected by Non-Tidal Atmospheric Loading. *Geofizicheskiy Zhurnal*, Vol. 45(1). https://doi.org/10.24028/gj.v45i1.275180.

[27] Kukhtar, D. and Oleskiv, R., (2024). Surface Deformations Analysis of Underground Gas Storage Using PSInSAR Based on Sentinel-1 Data. *Geodesy, Cartography, and Aerial Photography*, Vol. 100, 33–42. https://doi.org/10.23939/istcgcap2024.100.033.

[28] Du, Y., Yan, S., Zhao, F., Chen, D. and Zhang, H., (2022). DS-InSAR Based Long-Term Deformation Pattern Analysis in the Mining Region With an Improved Phase Optimization Algorithm. *Frontiers in Environmental Science*, Vol. 10. https://doi.org/10.3389/fenvs.2022.799946.

[29] Yi, Y., Xu, X., Xu, G. and Gao, H., (2023). Rapid Mapping of Slow-Moving Landslides Using an Automated SAR Processing Platform (HyP3) and Stacking-InSAR Method. *Remote Sensing*, Vol. 15(6). https://doi.org/10.3390/rs15061611.

[30] Wegmuller, U., Walter, D., Spreckels, V. and Werner, C. L., (2010). Nonuniform Ground Motion Monitoring With TerraSAR-X Persistent Scatterer Interferometry. *IEEE Transactions on Geoscience and Remote Sensing*, Vol. 48(2); 895–904. https://doi.org/10.1109/TGRS.2009.2030792.

[31] Sousa, J. J., Hooper, A. J., Hanssen, R. F., Bastos, L. C. and Ruiz, A. M., (2011). Persistent Scatterer InSAR: A Comparison of Methodologies Based on a Model of Temporal Deformation vs. Spatial Correlation Selection Criteria. *Remote Sensing of Environment*, Vol. 115(10); 2652–2663. https://doi.org/10.1016/j.rse.2011.05.021.

[32] Kim, T. T. H., Tran, H. H., Bui, K. L. and Lipeceki, T., (2021). Mining-Induced Land Subsidence Detected by Sentinel-1 SAR Images: An Example from the Historical Tadeusz Kościuszko Salt Mine at Wapno, Greater Poland Voivodeship, Poland. *Inżynieria Mineralna*, Vol. 1(2). https://doi.org/10.29227/IM-2021-02-04.

[33] Dorosh, L., (2021). *Monitoring of Technogenically Hazardous Objects by Means of Radar Interferometry.* [PhD Thesis]. Lviv: Lviv Polytechnic National University. (in Ukrainian).

[34] Pakshyn, M., Lyaska, I., Burak, K., Kovtun, V., Dorosh, L., Hrynishak, M., Mykhailyshyn, V. and Grytsyuk, T., (2019). Estimation of Earth's Surface Moves and Deformation of the Territory of Mine "Khotin" of Kalush-Golinskyy Field by Method of Radar Interferometry. *Geodesy and Cartography*, Vol. 45(1); 37–42. https://doi.org/10.3846/gac.2019.6300.

[35] Kukhtar, D., (2024). Analysis of Deformations of the Earth's Surface in the Area of the Kalush Mine Workings According to Radar Survey Data 2018–2022. *Modern Advances in Geodetic Science and Production*, Vol. 1(47); 110–117. www.doi.org/10.33841/1819-1339-1-47-110-117.

[36] Zhai, M., Liu, Q., Tao, Q. and Liu, G., (2023). SBAS InSAR Subsidence Monitoring for Mining Areas Based on Levelling Constraints. *Journal of Physics: Conference Series*, Vol. 2620(1). https://doi.org/10.1088/1742-6596/2620/1/012003.

[37] Li, J., Tan, Z., Zeng, N., Xu, L., Yang, Y., Siddique, A., Dang, J., Zhang, J. and Wang, X., (2025). Wavelet-Based Analysis of Subsidence Patterns and High-Risk Zone Delineation in Underground Metal Mining Areas Using SBAS-InSAR. *Land*, Vol. 14(5). https://doi.org/10.3390/land14050992.

[38] Chen, X., Chen, J., Wang, G., Zhang, Q. and Zheng, Y., (2025). Mining Subsidence Based on Integrated SBAS-InSAR and Unmanned Aerial Vehicles Technology. *Journal of Ocean University of China*, Vol. 24(1); 113–129. https://doi.org/10.1007/s11802-025-6009-6.

[39] Zhu, M., Yu, X., Tan, H., Yuan, J., Chen, K., Xie, S., Han, Y. and Long, W., (2024). High-Precision Monitoring and Prediction of Mining Area Surface Subsidence Using SBAS-InSAR and CNN-BiGRU-Attention Model. *Scientific Reports*, Vol. 14(1). https://doi.org/10.1038/s41598-024-80446-7.

[40] Yu, Z. and Huang, G., (2020). Using SBAS-InSAR to Detect Surface Movement above Old Mining Areas after Mine Closure. *IOP Conference Series: Earth and Environmental Science*, Vol. 502(1). https://doi.org/10.1088/1755-1315/502/1/012050.

[41] Delgado Blasco, J. M., Ziemer, J., Foumelis, M. and Dubois, C., (2023). *SNAP2StaMPS v2: Increasing Features and Supported Sensors in the Open Source SNAP2StaMPS Processing Scheme* (Version 2.0) [Computer software]. Zenodo. https://doi.org/10.5281/ZENODO.8362628.

[42] Yunjun, Z., Fattahi, H. and Amelung, F., (2019). Small Baseline InSAR Time Series Analysis: Unwrapping Error Correction and Noise Reduction. *Computers & Geosciences*, Vol. 133. https://doi.org/10.1016/j.cageo.2019.104331.

[43] Berardino, P., Fornaro, G., Lanari, R. and Sansosti, E., (2002). A New Algorithm for Surface Deformation Monitoring Based on Small Baseline Differential SAR Interferograms. *Geoscience and Remote Sensing, IEEE Transactions On*, Vol. 40; 2375–2383. https://doi.org/10.1109/TGRS.2002.803792.

[44] Doin, M. P., Lodge, F., Guillaso, S., Jolivet, R., Lasserre, C., Ducret, G., Grandin, R., Pathier, E. and Pinel, V., (2011). Presentation of the Small Baselin NSBAS Processing Chain on a Case Example: The Etan Deformation Monitoring from 2003 to 2010 Using Envisat Data. *Proceedings of the Fringe Symposium*. https://ens.hal.science/hal-02185213.

[45] Lanari, R., Mora, O., Manunta, M., Mallorqui, J. J., Berardino, P. and Sansosti, E., (2004). A Small-Baseline Approach for Investigating Deformations on Full-Resolution Differential SAR Interferograms. *IEEE Transactions on Geoscience and Remote Sensing*, Vol. 42(7); 1377–1386. https://doi.org/10.1109/TGRS.2004.828196.

[46] Kirui, P. K., Riedel, B. and Gerke, M., (2022). Multi-Temporal InSAR Tropospheric Delay Modelling Using Tikhonov Regularization for Sentinel-1 C-band Data. *ISPRS Open Journal of Photogrammetry and Remote Sensing*, Vol. 6. https://doi.org/10.1016/j.ophoto.2022.100020.

[47] Kennedy, J. H., Hogenson, K., Johnston, A., Kristenson, H., Lewandowski, A., Logan, T. A., Meyer, F. J. and Rine, J., (2021). Get HyP3! SAR Processing for Everyone. EGU General Assembly, EGU21-8973. https://doi.org/10.5194/egusphere-egu21-8973.

[48] Bekaert, D. P. S., Walters, R. J., Wright, T. J., Hooper, A. J. and Parker, D. J., (2015). Statistical Comparison of InSAR Tropospheric Correction Techniques. *Remote Sensing of Environment*, Vol. 170; 40–47. https://doi.org/10.1016/j.rse.2015.08.035.

[49] *ERA5 Hourly Data on Single Levels from 1940 to Present*. (n.d.). [Online]. Available: https://cds.climate.copernicus.eu/datasets/reanalysis-era5-single-levels?tab=overview. [Accessed: March 4, 2026].

[50] Macchiarulo, V., Milillo, P., Blenkinsopp, C., Reale, C. and Giardina, G., (2023). Multi-Temporal InSAR for Transport Infrastructure Monitoring: Recent Trends and Challenges. *Proceedings of the Institution of Civil Engineers - Bridge Engineering*, Vol. 176(2); 92–117.https://doi.org/10.1680/jbren.21.00039